Characterization of PM_2# $_5$ at a Traffic Site Using Several Integrated Analytical Techniques

X-RAY SPECTROMETRY

Characterization of PM2.5 at a Traffic Site Using Several Integrated Analytical Techniques

Journal:	*X-Ray Spectrometry*
Manuscript ID	XRS-20-0055.R1
Wiley - Manuscript type:	Research Article
Date Submitted by the Author:	n/a
Complete List of Authors:	Hamdan, Nasser; American University of Sharjah, Physics Alawadhi, Hussain; University of Sharjah, Applied Physics Department, X-ray Center for Material Analysis Shameer, Mohamad; University of Sharjah, Applied Physics Department, X-ray Center for Material Analysis, Research Institute of Sciences and Engineering
Keywords:	PM2.5, elemental analysis, chemical composition, Traffic site, X-ray spectroscopy

Characterization of $PM_{2.5}$ at a Traffic Site Using Several Integrated Analytical Techniques

Nasser M. Hamdan [1,2*], Hussain Alawadhi [2] and Mohamed Shameer [2]

[1] Physics Department, The American University of Sharjah, United Arab Emirates; nhamdan@aus.edu
[2] Center for Advanced Materials Research, University of Sharjah, United Arab Emirates halawadhi@sharjah.ac.ae
* Correspondence: nhamdan@aus.edu;

Received: date; Accepted: date; Published: date

Abstract: We have conducted a comprehensive, year-long, sampling campaign for particulate matter (PM) at a site near a major highway, following standard protocols. Total mass, elemental, and chemical composition of the fine fractions ($PM_{2.5}$) of particulates originating from traffic are determined using several complementary techniques. These complementary techniques include gravimetric analysis, X-ray fluorescence, scanning electron microscopy and energy dispersive spectroscopy, X-ray diffraction and black carbon multi-wavelength absorption. Conducting an enrichment factor analysis and correlation coefficient calculations on elements show that Si, Ca, Al, Fe, Ti, Mn, Mg, K, Na and Cr are of crustal origin, while P, Cl and V are enriched slightly from human activities. All other measured elements (Rb, Zr, Ba, Sr, S, Ni, Cu, Zn and Pb) have high enrichment factors and relate to anthropogenic sources. Sulfates in the form of Mascagnite and Koktaite had the largest contribution to $PM_{2.5}$ (43% of total PM concentration). Natural pollutants such as Quartz, Calcite, iron oxide, and aluminum oxide originating from the crust also contribute to $PM_{2.5}$. eBC and elements such as Zn, Ba, Cu, Fe and S are related to traffic emissions such as exhaust emissions and tire, brakes and road erosion. Correlation coefficients and enrichment factor calculations helped identify elements that are related to natural emissions and those related to anthropogenic sources. Being an arid region, the $PM_{2.5}$ mass concentrations were found to be within or slightly above international air quality standards.

Keywords: $PM_{2.5}$; elemental analysis; chemical composition; Traffic site; X-ray spectroscopy.

1. Introduction

The United Arab Emirates (UAE) has gone through rapid development and urbanization in the past few decades. It is characterized as an arid region with annual rainfall of less than 50 mm/year and large expansions of deserts [1, 2]. The country is associated with increased anthropogenic sources of pollution, including crustal materials due to mega construction projects, oil-related and industrial projects, and heavy traffic emissions. This is in addition to natural pollution sources such as sea salts from the Arabian Gulf and frequent dust storms originating from the desert. Outdoor particulate matter (PM) pollution is the leading environmental risk in the UAE due to its adverse health effects [3-13]. Furthermore, traffic emissions are a major source of anthropogenic pollutants that have adverse health effects. Several toxic elements and hazardous compound are emitted from fuel burning (diesel, gasoline and natural gas), tire and brake-pad erosion and road dust resuspension [14-17].

Although there have been several studies [3, 5, 10, 12, 18-23] in the region about the effect pollution can have on one's health, only a few publications involve comprehensive studies on the elemental composition, chemical speciation and source apportionment of $PM_{2.5}$ (particles with aerodynamic diameter less than 2.5 μm) and PM_{10} (particles with aerodynamic diameter less than 10 μm). Engelbrecht *et al.*, have conducted one of the major studies on characterizing mineral dust and other aerosols in the Middle East [19, 24]. Their study was part of the Enhanced Particulate Matter Surveillance Program (APMSP) [20], and was done on behalf of the US Department of Defense for

John Wiley & Sons
https://doi.org/10.1002/xrs.3201

five deployment countries at fifteen US military sites in the Middle East. The countries involved in this program are Iraq, Kuwait, Afghanistan, Qatar, and the UAE. Although this study involved comprehensive sampling and characterization work, it only investigated samples collected from military bases in the desert, far from urban and residential areas. The study used only one site in Qatar, one site in the UAE, four sites in Kuwait and six sites in Iraq. They found that the 24-hour mean mass concentration of $PM_{2.5}$ in the UAE site was 52 μg/m^3. They also identified various minerals in $PM_{2.5}$ and PM_{10} at all these sites and concluded, using X-ray diffraction (XRD), scanning electron microscopy and energy dispersive spectroscopy (SEM/EDS) analysis, that the mineral content of the aerosols is originating from local soil. Urban and residential areas are more susceptible to industrial and traffic pollution. Therefore, and despite the importance of this study, it does not provide information about anthropogenic pollutants in the region. The second comprehensive study about long-term trends in the ambient fine PM in the UAE was conducted by Al Taani *et al*. [21]. They used satellite data from 1980 to 2016 to study long-term contribution of $PM_{2.5}$ in the UAE and reported an overall average of $PM_{2.5}$ mass concentration of 61.2 μg/m^3, with annual averages varying between 77 to 45 μg/m^3. The study did not include any elemental or chemical analysis of the $PM_{2.5}$ components nor did it include any attempt for source apportionment. In a review article, Tsiouri *et al.* have summarized the available source apportionment studies of atmospheric PM in the Middle East [7]. In their study, they have recognized significant problems in quantifying PM emissions in the region. They have also concluded that there is a need for a systematic data collection, source apportionment and assessment of PM levels to help minimize adverse health effects. Reid *et al.*, have performed the United Arab Emirates Unified Aerosol Experiment (UAE^2), which is an atmospheric thermodynamic and aerosol data collection on 18 flights in the UAE between August to September 2004 [25]. They observed high regional dust from 100 to 300 μg/m^3 in the background and more than 1.5 mg/m^3 during dust events in the first 5 km of the atmosphere. They also observed 10 to 100 μg/m^3 of sulfate-based pollutants originating from the region's petroleum industry.

There have been several other attempts to study various aspect of PM pollution in the region. For example, Al-Salem *el al*. [26] have performed a two-year study of PM_{10} in an urban site in Kuwait. They reported a mean annual mass concentration for PM_{10} of 290 μg/m^3 for 2004 and 2005. Al Katheeri *et al*., conducted a study of gaseous and PM ambient pollutants at a site that has four gas turbines in the UAE. They reported that the 24 h average of PM_{10} mass concentration was 150 μg/m^3 using the Beta attenuation technique at an Ambient Air Monitoring station (AQMS) [18]. Arashiro and Leith have used a passive personal sampler to study the size distribution and mass concentrations of $PM_{2.5}$ and $PM_{(10-2.5)}$ in the UAE and concluded that these passive samplers can provide reasonably precise measurements [23]. They have attempted to demonstrate the potential of using WRF-Chem to estimate the air quality index (AQI) over the UAE along with two satellite products (MODIS-MAIAC and MSG-SEVIRI) for dust detection and tracking. Al-Thani *et al*., have conducted a preliminary study on 9 samples of fall-out dust in Doha, Qatar collected in 2016 [22]. They used SEM and optical microscopy to study the morphology and shape distribution of particles and estimated the average particle size to be 7.4 μm. Alattar and Yousif have proposed a comparative study to identify the impact of air pollution, including PM levels, on health in the Arab World and in Oman in particular [27]. They also suggested mathematical models to predict pollution levels using a fast, cheap and safe method.

In the past, we have conducted several studies for outdoor [1, 8, 28-30], and indoor [8] PM using complementary analytical techniques. However, our current study is a systematic sampling campaign and analytic approach utilizing several non-destructive, bulk and spectroscopic techniques to identify the constituents of the fine fraction of PM in the air ($PM_{2.5}$) at a "traffic" site. The study includes gravimetric and statistical analysis, complementary non-destructive techniques such as X-ray fluorescence (XRF), SEM/EDS, XRD, and black carbon content measurements to determine elemental composition and chemical speciation for PM, that can be used as source tags for pollutants [31].

2. Experiments

2.1. Sampling campaign and protocol

Sampling was performed using a low volume sampler LVS/LVS6-RV manufactured by Sven Leckel, Ingenieurbüro GmbH Germany. $PM_{2.5}$ samples were collected for 24 hours every sixth day between October 26, 2017 and January 14, 2018, followed by sampling twice a week every Tuesday (a working day) and Friday (a weekend day) until October 26, 2018, from 00:00 to 23:59. EN standard (EN12341, 2.3 m^3/h) on 47 mm diameter Teflon filters was used, with size-selective jets of 2.5 µm. The sampling site is located near Sharjah International Airport highway with coordinates: 25°20′39.2″N and 55°26′46.4″E. Figure 1 shows the map of the sampling site. The location is an air quality-monitoring site for the Sharjah-based Bee'ah, an environmental management company. The site is within 50 meters of the highway and about 15 m above the highway level. The highway usually has high traffic congestion in the morning between 7:00 and 9:00 am, and in the evening between 4:30 and 8:00 pm on weekdays, while it has normal traffic flow outside these intervals and during weekends. The temperature and humidity were recorded every five minutes during sampling. A normalized air volume at standard temperatures, pressures and humidity was then used to calculate the amount of $PM_{2.5}$ per cubic meter of air. Due to high temperatures in the region, the normalized air volume was usually about 10% less than the measured air volume. The normalized volumes were used for all the subsequent calculations. Airborne $PM_{2.5}$ mass concentrations were determined gravimetrically following a standard operating procedure [1]. Teflon filters were preconditioned at standard temperatures (23 °C) and relative humidity (RH) of 55%, neutralized with an electrostatic charge neutralizer, and weighed on a Sartorius microbalance (model CPA2P) with a precision better than 1 µg. The average of four weighing measurements were taken to be the mass of the filter before sampling. The process is repeated after sampling to calculate the mass concentrations. The air volume during sampling was normalized by continuously (every five minutes) monitoring the relative humidity, pressure and temperature using meteorological sensors attached to the sampling head.

2.2 Equivalent black carbon measurements

To determine the equivalent black carbon (eBC) [1, 32], a Multi-wavelength Absorption Black Carbon Instrument (MABI) was used. The instrument uses 7 lasers to determine the light absorption coefficient of a specimen at different wavelengths. "The Laser absorption method relies on a mass absorption coefficient, which is a strong function of the particle size, refractive index and density of the eBC particles, as well as the wavelength of light used. The eBC data were not corrected for the contribution of hematite. As fine eBC can be generated from a range of different sources, its particle size and density distribution may also vary in a collected sample depending on the dominant sources of eBC at the site" [33].

2.3. XRF: Elemental analysis

XRF measurements were performed using a Thermofisher QuantX spectrometer, with Rh tube source and using 8 mm beam size to obtain good averaging of the data. The spectrometer is equipped with eight source-filters that are used for specific elements.

Micromatter thin film standards, with film thicknesses comparable to sample thicknesses, were used to establish single-point calibration values for the sensitivity factors (in cps mA^{-1} μg^{-1} cm^2) for the following elements: Na, Mg, Al, Si, P, S, Cl, K, Ca, Ti, V, Cr, Mn, Fe, Ni, Cu, Zn, Rb, Sr, Zr, Ba and Pb. Next, elemental composition (in $\mu g/m^3$) for all the filters was determined using the calculated sensitivity factors. For the purpose of quality assurance and control, the data was validated against a NIST Standard Reference Material 2783, using the same established calibration procedures mentioned above for the Micromatter film standards. This Standard Reference Material is an air particulate sample reduced in particle size to simulate airborne $PM_{2.5}$ and deposited on a polycarbonate filter membrane [1].

2.4. SEM/EDS measurements

Imaging and elemental mappings were performed for selected filters on a TESCAN environmental scanning electron microscope (VEGA3 XMU) using an Oxford Instruments X-Max 50 EDS detector. Mappings were done for 8 minutes. Samples representing different weather conditions and different seasons were selected for analysis. The electron beam excitation was set at 20 kV and low vacuum (10 Pa) was used to avoid charging of the filters. Fourteen filters from both clear and dusty days were selected for SEM imaging and elemental mapping.

2.5. XRD crystallographic phase analysis

X-ray diffraction measurements were performed on selected filters using a Bruker D8 ADVANCE system with a Cu tube and a linear detector (LYNXEYE XE). More than twenty samples of $PM_{2.5}$ were selected for XRD analysis. The measurements were performed with a step size of 0.02°, 2θ range of 5° to 55°, and time per step of 2.5 s. After background removal, the different phases were identified using the ICDD database PDF-4+ (Release 2019). The same filters that were used for SEM/EDS analysis, from both clear and dusty days and for different seasons, were selected for XRD analysis.

3. Results and Discussions

3.1 $PM_{2.5}$ mass concentrations

Figure 2 represents the mass concentrations in $\mu g/m^3$ for each of the $PM_{2.5}$ filters collected over the sampling campaign period. Other than dust storm and windy days, the mass concentrations lie within or slightly higher than international air quality standards. The United States Environmental Protection Agency's National Ambient Air Quality Standards (NAAQS) for 24-hour fine-particle mass concentration is 35 $\mu g/m^3$, while the WHO standard guideline is 25 $\mu g/m^3$. The $PM_{2.5}$ data show that during winter (November to February) several values lie within the international standards, with an average mass concentration of 36 ± 11 $\mu g/m^3$. More dusty days start to occur during the spring and summer, resulting in larger $PM_{2.5}$ concentrations with an average of 52 ± 17 $\mu g/m^3$. The overall mass concentration average was (48 ± 7) $\mu g/m^3$. Although natural pollutants originating during dust events contribute mainly to the coarse fraction of PM (between 2.5 and 10 µm), they also contribute to the fine particles (less than 2.5 µm) in the atmosphere. Table 1 shows 15 dust events that occurred during the sampling period, with one severe dust episode on July 31, 2018. The $PM_{2.5}$ concentration on that day was 146 $\mu g/m^3$, while that of PM_{10} concentration was 676 $\mu g/m^3$. The table shows that most dust events occur during the months of May-August. The UAE climate during the year can be divided into two seasons: a very hot summer and a moderate "winter". We can consider the months between May and October to be the summer season, where both the temperatures and humidity are high, while the months between November and March are more moderate. Table S1 shows the average meteorological parameters in Sharjah between 1977 and 2019 [2].

Zalakeviciute *et al*. reported a positive correlation between $PM_{2.5}$ and RH in urban traffic areas associated with low precipitation (< 1mm per day) or rain-free days [34]. They even concluded that daily averages of $PM_{2.5}$ were above healthy limits in Belisario, an area known for high RH. Cheng *et al*. have also reported that high concentrations of $PM_{2.5}$ during summer were typically associated with high RH [35]. In the presence of high RH and low precipitation in Sharjah, fine particles remain suspended in the air for prolonged periods, resulting in higher mass concentrations in the spring and summer months. This is also evident from the hazy atmosphere during these months with an average annual visibility in Sharjah of 9 km [36] .

3.2: Equivalent black carbon

Figure 3 shows the variation of eBC concentrations for $PM_{2.5}$ at different sampling dates, obtained using the MABI instrument. The average eBC over the campaign period was 6.5 μg/m^3 (13.6% of the total PM), with values ranging from 5% on November 25, 2017, to 25% on April 10, 2018. Traffic emission, fossil fuel burning in energy generation, residential and industrial emissions (including petroleum industry) are believed to be the main sources of eBC [37, 38]. We found a statistically significant positive correlation with a correlation factor of 0.48 between eBC concentration and $PM_{2.5}$ concentration with $p < 0.001$.

3.3 XRF results

XRF measurements were performed on all the 86 collected $PM_{2.5}$ samples. Twenty-two elements were analyzed, and their mass concentrations and uncertainties were determined. Since these elements do not exist in pure elemental state, they are usually reported as oxides [39]. Nevertheless, based on our XRD and EDS results below, S appears mostly as Mascagnite [$(NH_4)_2SO_4$], which is the dominant phase in almost all the samples. Therefore, in our calculations, we have taken Mascagnite to represent S. Supplementary Table S2 shows the concentrations of all elements within the detection limits. Sheet 1 shows the concentration of the oxides of most elements (except for S and Cl), while sheet 2 shows the elemental concentrations. Table S3 shows the lower detection limits (LDL) for the elements measured in this work, as obtained with our QuantX machine.

Table S2 shows that sulfates (present mainly as Mascagnite) represent the largest fraction of the total $PM_{2.5}$ (> 40%) among all other constituents, with an annual average of 20.6 μg/m^3, and with values ranging between 4.4 and 52.6 μg/m^3. These results indicate that sulfates, which are secondary pollutants formed from gas-to-particle conversion in the atmosphere, are the dominant phases in $PM_{2.5}$ [40, 41]. The average mass concentration of sulfates in the winter and summer are 17.4 μg/m^3 and 22.0 μg/m^3, respectively. The table also shows that Ca (taken as CaO) has an average mass concentration over the sampling year of 4.5 μg/m^3. The average values for Ca in the winter and summer were 2.8 μg/m^3 and 5.9 μg/m^3, respectively. Similar behavior of lower mass concentrations in the winter compared to summer is also observed for other major natural pollutants such as Fe, Si and Al. All these results agree with the observed total PM concentrations in the two seasons. More dust storms take place between April and September, resulting in increased pollution levels. Furthermore, precipitation in winter (despite its low rate) contributes to the wet deposition of fine dust that may otherwise remain suspended for prolonged periods. Summer in the UAE is a very hot and humid season, with practically zero precipitation. Figure 4 shows the variation of the mass concentrations of Mascagnite, eBC, Quartz, CaO and iron oxide (Fe_2O_3) over the whole year of sampling.

Sea salts originating from the sea breeze blowing from the Arabian Gulf are among the natural sources of PM in the region. There is a reasonable correlation (~ 0.54) between the concentrations of Cl and Na for the data collected over the sampling campaign. High correlations between Na and Cl were observed for several days such as February 20, and July 6, 2018. The measured correlation factor is expected because not all the Na content is correlated with Cl. For example, there is volatile loss of Cl compounds and formation of Na_2SO_4 aerosols by the heterogeneous reaction of NaCl aerosol and H_2SO_4 vapor. Some of the Na contribution is due to formation of sodium nitrates ($NaNO_3$), as will be shown below from elemental maps and XRD results. The presence of aged sea salts is due to the depletion of Cl. Fresh sea salt exists mostly in the coarse fraction of PM [42]. The percentage of the fresh to aged sea salt will be determined by a future project using PM_{10}. The presence of other crustal elements with lower concentrations, such as Mg, K, Mn, Cr, and Ti, are also confirmed from XRF and will be discussed in terms of enrichment factors below.

XRF analysis also revealed the presence of trace elements such as Ni, V, Pb, Zn and Cu. These elements can be used as markers for certain pollution sources. For example, V and Ni are known to be originating from heavy oil combustion used in ships and industries [42-45]. Other industries such as oil related industries in the region may also contribute to the emission of V and Ni [46, 47]. Figure 5 shows a good correlation (> 0.75) between these two elements, indicating that they are mostly originating from the same source. The V (in the form of vanadium oxide) concentrations varied between (10 – 70) ng/m^3, while the Ni (in the form of Nickle oxide) concentrations varied between (2 – 30) ng/m^3. Zn, Cu, Ba, Mn, eBC and Pb are associated with traffic emissions [14, 15, 48, 49]. Other crustal elements such as Fe, Al, Si and Ca are also considered to be due to traffic through road dust resuspension [14, 15, 49]. Figure 6 shows the variation of Pb content for all sampling days. The figure shows an average mass concentration of lead oxide of 30 ng/m^3 with a few values spiking as high as 190 ng/m^3. Lead is originating from industrial emissions, such as a few car battery recycling plants that are located within a few miles of the sampling site. These values are still well below the EU air quality limits of 500 ng/m^3 [48].

Table 2 shows the correlation among the mass concentrations of the measured elements. There is a significant correlation between highlighted elements in the table with Pearson coefficient $p < 0.05$. The table shows a strong correlation among Al, Ca, K, Fe, Ti and Mn (with correlation factors above 0.9). These elements also correlate well with Cr, P and Rb. These high correlation factors imply that these elements are of common crustal origin. This result will be confirmed from enrichment factor calculations below. The slightly lower correlations among Cr, P, Rb and the other crustal elements mentioned above indicates that these three elements have partly anthropogenic contributions in $PM_{2.5}$. In contrast, S has negative correlations with all elements except V and Ni (with correlation factors of 0.4 and 0.25, respectively) and lower positive correlation with Rb, Cr and Zn. These results confirm that S is mainly an anthropogenic pollutant and Rb and Cr have small anthropogenic contributions. Pb has very low or negative correlations with several elements except Cu, Zn, Ba and Zr. The strong correlation between V and Ni (0.75) shows that they are mostly originating from the same source in agreement with the literature [50]. Several source apportionment studies assign the emission of V and Ni to heavy oil combustion [14, 49]. Mazzei *et al.* have reported that heavy oil combustion is identified by the concentration ratio of V : Ni of 3.2 ± 0.8 [45]. Nigam *et al.* have measured the concentration ratio of V : Ni of different ship engines and fuels by sampling directly at the exhausts of the auxiliary engines used by these vessels and found it to be in the range of 3.5 to 4 [51]. The average value of the V: Ni concentration for our sampling period is 2.9 ± 0.7. Hence, we assign the observed concentrations of V and Ni to heavy oil combustion from ships in the nearby Sharjah port, which is about 4 km from the sampling site. Ba, Zn, Fe and Cu, in addition to eBC are usually associated with traffic emissions that include exhaust emissions, brake lining abrasion (Cu and Ba), metallic brakes and rubber wear of tires (Zn, Fe and eBC) [14, 49, 52, 53]. Traffic emissions also include Ca, Fe, Al, Si and carbon from road surface wear and road dust resuspension. S is a major pollutant that is present as a secondary phase (Mascagnite) resulting from the conversion of SO_2 gas originating from fossil fuel burning into sulfate particulates. Thus, it can also be associated with the exhaust emission, power plants and industrial emissions [1]. Na and Cl come from the sea salt that is transported with the sea breeze from the nearby Arabian Gulf, which is about 4 km from the sampling site. Although Mg can come either from the sea salt or from crustal materials [49], we believe that in our case it is mostly a crustal element because of its high correlation with other crustal elements mentioned above. Mg also has a low enrichment factor (EF) of 3.9 and 3.5 for the cold and hot seasons, respectively, as discussed below. Furthermore, there is a low, but statistically significant positive correlation between Mg and Na with correlation factor of 0.3 and $p < 0.006$. The ratio of Mg/Na in sea water is in the range of 0.15 [54], while, in our $PM_{2.5}$ samples it ranges from 0.44 to 12 with an average value of 2.6, indicating mostly a crustal origin for Mg.

Enrichment factors can be used to distinguish between natural and anthropogenic origin of elements, by showing the degree of enrichment of certain elements compared to the relative abundance of these elements in the crustal material. EF is a quantitative approach for evaluating the strength of the crustal and noncrustal origin by calculating the concentration of a certain element relative to a reference crustal element that is abundant in the earth's crust. Reference elements are usually Al, Si and Fe [55, 56]. The EF for element X is defined in the following equation [57, 58]:

$$EF_X = (X/Y)_{air}/(X/Y)_{crust} \quad , \tag{1}$$

where Y is the concentration of the reference element, which in our case is Si. A high enrichment factor for a certain element suggests a prevailing anthropogenic origin. If the EF large for a certain element, then the element is not enriched, and the main source is natural, such as soil or rock weathering. If the EF is small, then the primary source is anthropogenic [58, 59]. The elemental composition of the crust were obtained from references [60, 61].

Figure 7 (a, b) shows the enrichment factors for various elements relative to Si, both for the cold season (October 15 – April 1, 2018) and for the hot season (April 1 – September 15, 2018). We can classify the elements into three groups: not enriched (EF < 10) , moderately enriched (10 < EF < 100), and highly enriched (EF > 100). Figure 7 shows that Mn, Al, K, Ti, Fe, Mg, Cr and Ca have low EF (< 10) for both the cold and the hot seasons, indicating their crustal origin. The second group is P, V and Cl, which are moderately enriched by human activities. The third group of elements consists of Rb, Zr, Ba, Sr, S, Ni, Cu, Zn and Pb, which are highly enriched. As explained above, these elements are associated with traffic emissions (exhaust emission, road dust resuspension, road erosion and break and tire wear), oil combustion, power plants and industrial emission. It is obvious that the enrichments of P, V, Cl, Rb, Zr, Ba, Sr, S, Ni, Cu, Zn and Pb are higher in the cold season than the hot season, showing the significance of anthropogenic sources in winter. Summer in the Gulf region in general, including the UAE, is associated with lower human activities. The majority of the UAE population leaves the country for summer vacation, escaping the high temperatures and humidity [62]. Furthermore, schools are closed, and many businesses and human activities operate at their minimum capacities, which lead to a drastic drop in the number of vehicles on the roads and in the energy consumption. All these factors lead to the observed increase in the EF of anthropogenic pollutants in winter compared to summer. Pb was the highest enriched element followed by Zn. EF of Pb in the winter and summer were 30700 and 8650, respectively, indicating that it is originating from a major human activity. Gasoline has been Pb-free for a long time in the region and most vehicles are relatively new. We found out that Pb is originating mainly from several car battery recycling plants nearby. Table 3 shows the mass concentration of Pb collected from the premises of one of these plants during two working days and a weekend day. The table shows high concentrations of Pb during the working days compared with the weekend.

XRF results give an average of 4.9 μg/m^3 for the mass concentration of S. Assuming that S is present mostly in the form of the dominant Mascagnite phase, this value corresponds to a mass concentration of 20 μg/m^3 for Mascagnite. Hence, on average, Mascagnite represents about 43% of the $PM_{2.5}$ total mass concentration (48 μg/m^3). The remaining inorganic species identified by XRF, which are taken to be oxides, add up to 13 μg/m^3, representing 28% of the total, while the eBC (obtained from MABI instrument) is about 14%. Although the 28% inorganic species include both natural and anthropogenic sources, most of this fraction is due to natural sources. The unaccounted mass, which is about 15%, is probably composed mostly of organic matter and water, which was ignored in the above calculations. We estimate the error in the measurement to be in the range of 15 to 20%. Figure 8 shows the distribution of various contributions to $PM_{2.5}$ average mass concentrations based on the techniques used in this study.
Organic carbon (which is not detected by techniques used in this study) can come from both primary and secondary sources. These aerosol pollutants are expected to be high in the vicinity of an active traffic highway. Alkanes are among the most abundant organic species [63]. Other common organic compounds originating from road traffic emissions, solid fuel combustion and industrial emissions are polycyclic aromatic hydrocarbons (PAHs) [64]. Biologic and soil organic matter, and organic acids are also reported in the literature as common organic PM [63]. Pant *et al*. have reported in their study for New Delhi that organic matter contributes to more than 33% of $PM_{2.5}$ in the summer [63]. Fu *et al*. [65] have reported, based on organic tracers, that traffic contributions can be as high as 43%. Our estimated values for organic carbon are less than these reported values. It should be noted that evaluation of elemental concentrations using XRF analysis is usually associated with several uncertainties. Among them is the inability to detect lighter elements such as O, C, and N. XRD and EDS results indicate the presence of several minerals as major phases in the samples such as Koktaite, Gypsum, Palygorskite and sodium nitrate, with large fractions of these lighter elements. In addition, experimental and systematic errors in gravimetric analysis and eBC measurements, also contribute to the uncertainty in the overall identification of various pollution sources.

3.4. XRD Results

Although XRD is not commonly used in PM analysis, we have utilized this method efficiently to identify major crystallographic phases present in both $PM_{2.5}$ and PM_{10} [28]. XRD analysis was performed on 20 selected samples. Figure 9 is a representative of most of the analyzed samples. The figure shows the analysis of filter 80, sampled on October 5, 2018. Although this was a dusty day with a mass concentration of 77 μg/m^3, the XRD pattern does not show any crustal or mineral phases. The figure shows the presence of two phases: ammonium sulfate as Mascagnite, and calcium ammonium sulfate [$(NH_4)_2Ca(SO_4)_2 \cdot H_2O$] as Koktaite, in addition to peaks originating from the Teflon filter. Most of the analyzed samples showed only these three phases. This is a strong evidence that sulfates are the dominant phase in the fine PM, which agrees with the observed XRF results and analysis above. It should be noted that although XRD cannot detect trace, organic or amorphous phases, it is a very powerful tool to understand the composition and formation mechanisms of secondary pollutants. Masganite and Koktaite exist in very fine particle sizes [8]. Mascagnite is a secondary pollutant formed by the conversion of sulfur dioxide gas from fossil fuel burning in traffic, power plants and various industries to fine particles. Although the Diesel used in the UAE has low sulfur content (10 ppm), this sulfur content reaches up to 500 ppm in some of the neighboring Gulf Countries [66]. With the high temperatures, abundance of sunshine, and high relative humidity in Sharjah, oxidation of the SO_2 gas by hydroxyl radicals (OH) produces sulfuric acid (H_2SO_4), which then interacts with ammonia (NH_3) to form fine particles of ammonium sulfate (< 0.5 μm in diameter) that can travel hundreds of kilometers in the atmosphere *[67]*. Furthermore, natural gas that has high sulfur content is the main source of energy used in power plants in the UAE in recent years [68]. Calcite that is present in the atmosphere reacts with the ammonium sulfate, at a rate measured in days, to yield Koktaite as an intermediate product and, finally, Gypsum [$CaSO_4 \cdot 2H_2O$]. Gypsum appears mostly in PM_{10} *[39, 69]*.

Crustal and mineral phases were only observed in the XRD results of very few samples. Figure 10 shows the XRD pattern of sample 35, collected on April 17, 2018, a dusty day. In addition to Koktaite and Mascagnite, Quartz, Gypsum and Calcite are the major three phases in this sample. Other phases present in this sample are: Palygorskite [$(Mg,Al)_2Si_4O_{10}(OH)\bullet_4(H_2O)$],) and Chlorite-serpentine [$(Mg,Fe)_6AlSi_3O_{10}(OH)_8$], a mineral consisting of magnesium and iron silicates that have similar layered crystal structure as Chlorite. Halite [NaCl] and sodium nitrate [$NaNO_3$] were not detected by XRD but have been observed in the EDS maps. An example is shown in the next section.

3.5. SEM/EDS Results

SEM images, EDS spectra and elemental maps were obtained for several samples. Figure 11 shows the SEM image and elemental maps on part of filter 80 (corresponding to the XRD pattern in figure 9). The SEM micrograph shows the presence of a large agglomeration of crystals, with one having a size of more than 25 µm. Elemental maps show an excellent correlation between the maps of S, N and O, confirming the results observed by XRD above and the domination of S in the XRF results. This is also a confirmation that S exists as a sulfate phase, a secondary phase that is formed in the atmosphere through gas-to-particle conversion, as explained earlier. The figure also shows maps of F and C, both representing the filter material. These elements are clearly absent in areas where ammonium sulfate exists.

The critical RH for ammonium sulfate at 24 °C is 81%. On October 6, from 00:00 to 9:00 am, the sample was left outside under the ambient atmosphere with wide swings in humidity and temperature. RH increased from 89% to 100% and the temperature dropped to 24 °C, causing some of the Mascagnite on the filter to deliquesce. As the sun rose later in the day, the humidity decreased to 29% while the temperature increased to 37 °C, causing evaporation of the moisture and formation of the observed large chunks of ammonium sulfate (~ 25 µm x 15µm) in figure 11.

Koktaite was also observed in different regions of $PM_{2.5}$ samples. It was even observed in the PM_{10} sample that was collected simultaneously with the $PM_{2.5}$ filter 80 above, confirming the XRD results. Figure 12 shows the SEM micrograph and SEM elemental maps for parts of PM_{10} filter 67 that was sampled simultaneously with filter 80. The figure shows the formation of long rods that have good correlations in the elemental maps of Ca, S, N and O, indicating formation of the Koktaite phase observed by XRD.

The EDS maps of most samples also show correlations among several other elements (not shown here) that were measured by XRF and correspond to mineral phases observed by XRD, such as Quartz, Calcite, Palygorskite and Chlorite-serpentine. In addition to maps for the phases observed by XRD, Halite and sodium nitrate have been observed in the EDS maps of several samples. Figure 13 shows elemental maps of Na, Cl, N and O for sample 21, which was collected on February 20, 2018. The white crystal on the upper right corner in the SEM image is a Halite crystal, as indicated by the good correlation between Na and Cl (and no correlation with O). For several other smaller crystals, Na correlates well with both N and O, indicating the presence of sodium nitrate. February 20, 2018 was a clear day and the mass concentration of $PM_{2.5}$ was 42 µg/m^3. Based on the direction of the wind, the Halite in this sample is originating from the sea breeze coming from the Arabian Gulf (to the west of the sampling site), while the sodium nitrate is a secondary pollutant formed in the atmosphere.

4. Conclusions

Fine PM sampled at a roadside site were found to be affected by dust events and traffic. XRF results show that S has the highest contribution of all measured elements in $PM_{2.5}$ samples. Enrichment factor analysis reveal that Si, Fe, Ca, Al, Mg, K Mn, Na, Ti and Cr are crustal elements, with EF < 5 while P, V and Cl are partially enriched with EF > 10. Rb, Zr, Sr, S, Cu, Ni, Ba, Zn and Pb are highly enriched, due to their anthropogenic nature. The EFs for anthropogenic elements are higher in winter than in summer, due to a reduction in human activities in the summer. We have also observed high correlations among Si, Ca, Fe, Al, Mg, K, Mn, and P, confirming the crustal origin of these elements. A medium correlation was observed between Na and Cl originating from fresh and aged sea salts. Ba, Zn, Fe and Cu, in addition to eBC are traffic related elements. The high correlation coefficient between V and Ni shows that they are mostly originating from heavy oil combustion emissions from ships and power plants. A summary of the source tags of different elements is shown in Table 4.

XRD and EDS results indicate that sulfates are secondary pollutants that exist mainly in the form of Mascagnite and Koktaite, the two dominate phases in $PM_{2.5}$. XRD and EDS results also show the presence of fresh (Halite) and aged (sodium nitrate) sea salts. Several minerals were also identified by XRD, including Quartz, Calcite, Gypsum, Palygorskite and Chlorite-serpentine. eBC is found to constitute an average of about 14% of the total $PM_{2.5}$ mass and is due to traffic, energy generation and industrial emissions. Based on the mass balance approach, sulfates represent 43% of $PM_{2.5}$, other inorganic compounds (both natural and anthropogenic) represent 28%, eBC 14% and the remaining 15 % are due to organic carbon compounds. In the absence of dust storms, the mass concentrations of $PM_{2.5}$ were found to be within international standards. The integration of complementary, nondestructive analytical techniques such as gravimetric analysis, eBC, XRF, XRD, and SEM/EDS mapping enabled us to perform chemical speciation and analysis to identify various primary and secondary compounds in the atmospheric fine PM and their origin.

The techniques used in the present study lack the capability to determine the organic and ionic components of the PM. Future work will include performing quantitative source apportionment for both $PM_{2.5}$ and PM_{10} that are sampled simultaneously using the same protocols.

Supplementary Materials: The following are available online at www.mdpi.com/xxx/s1. Table S1: The average meteorological parameters in Sharjah for the period 1977-2019; Table S2: Elemental compositions with their uncertainties, Table S3: The lower Detection Limits of the used XRF system for the measured elements.

Author Contributions: All the authors have contributed to this article as follows: methodology, NMH and HA; software, MS; validation, NMH and HA; formal analysis, NMH and HA; investigation, NH and MS; data curation, MS, HA, NH; writing—original draft preparation, NMH.; writing—review and editing, HA and NMH.; supervision, NMH; project administration, NMH; funding acquisition, NMH and HA. All authors have read and agreed to the published version of the manuscript,

Funding: This work was funded by the American University of Sharjah under grant number FRG16-R-08, and by the University of Sharjah under grant number No. 16020143026-P.

Acknowledgments: The authors acknowledge the support of the Advanced Materials Research Lab at the University of Sharjah. NMH received support from the Dean's office, College of Arts and Sciences at the American University of Sharjah. The work in this paper was supported, in part, by the Open Access Program from the American University of Sharjah.

Conflicts of Interest: The authors declare no conflict of interest.

References

[1] N. M. Hamdan, H. Alawadhi, N. Jisrawi, and M. Shameer, "Characterization of fine particulate matter in Sharjah, United Arab Emirates using complementary experimental techniques," *Sustainability*, vol. 10, p. 1088, 2018.

[2] NCMS. (2019). *UAE climate yearely report 2003- 2018*. Available: https://www.ncm.ae/en/climate-reports-yearly.html?id=8805

[3] J. M. Gibson and Z. S. Farah, "Environmental risks to public health in the United Arab Emirates: a quantitative assessment and strategic plan," *Environmental health perspectives*, vol. 120, pp. 681-686, 2012.

[4] J. Al Jaberi, J. Thomsen, M. Al Hashimi, S. Al Bagham, M. Al Yousuf, K. Jamil, *et al.*, "The national strategy and action plan for environmental health for the UAE," *Abu Dhabi*, 2010.

[5] Y. Li, J. M. Gibson, P. Jat, G. Puggioni, M. Hasan, J. J. West, *et al.*, "Burden of disease attributed to anthropogenic air pollution in the United Arab Emirates: estimates based on observed air quality data," *Science of the total environment*, vol. 408, pp. 5784-5793, 2010.

[6] C. M. Wong, H. Tsang, H. K. Lai, G. N. Thomas, K. B. Lam, K. P. Chan, *et al.*, "Cancer mortality risks from long-term exposure to ambient fine particle," *Cancer Epidemiology and Prevention Biomarkers*, vol. 25, pp. 839-845, 2016.

[7] V. Tsiouri, K. E. Kakosimos, and P. Kumar, "Concentrations, sources and exposure risks associated with particulate matter in the Middle East Area—a review," *Air Quality, Atmosphere & Health*, vol. 8, pp. 67-80, 2015.

[8] N. M. Hamdan, H. Alawadhi, N. Jisrawi, and M. Shameer, "Size-resolved analysis of fine and ultrafine fractions of indoor particulate matter using energy dispersive X - ray fluorescence and electron microscopy," *X-Ray Spectrometry*, vol. 47, pp. 72-78, 2018.

[9] K. A. Miller, D. S. Siscovick, L. Sheppard, K. Shepherd, J. H. Sullivan, G. L. Anderson, *et al.*, "Long-term exposure to air pollution and incidence of cardiovascular events in women," *New England Journal of Medicine*, vol. 356, pp. 447-458, 2007.

[10] H. A. Hochstetler, M. Yermakov, T. Reponen, P. H. Ryan, and S. A. Grinshpun, "Aerosol particles generated by diesel-powered school buses at urban schools as a source of children's exposure," *Atmospheric environment*, vol. 45, pp. 1444-1453, 2011.

[11] A. Bener, M. Dogan, M. Ehlayel, N. Shanks, and A. Sabbah, "The impact of air pollution on hospital admission for respirarory and cardiovascular diseases in an oil and gas-rich country," *European annals of allergy and clinical immunology*, vol. 41, p. 80, 2009.

[12] J. M. Gibson, J. Thomsen, F. Launay, E. Harder, and N. DeFelice, "Deaths and medical visits attributable to environmental pollution in the United Arab Emirates," *PloS one*, vol. 8, p. e57536, 2013.

[13] A. Nemmar, S. Al-Salam, S. Zia, S. Dhanasekaran, M. Shudadevi, and B. H. Ali, "Time-course effects of systemically administered diesel exhaust particles in rats," *Toxicology letters*, vol. 194, pp. 58-65, 2010.

[14] I. Sundvor, N. Balaguer, M. Viana, X. Querol, C. Reche, F. Amato, *et al.*, "Road traffic's contribution to air quality in European cities," *ETC/ACM technical paper*, vol. 14, pp. 1-74, 2012.

[15] I. Sundvor, N. Castell Balaguer, M. Viana, X. Querol, C. Reche, F. Amato, *et al.*, "Road Traffic's Contribution to Air Quality in European Cities, ETC/ACM Technical Paper 2012/14," *Copenhagen: European Topic Centre for Air Pollution and Climate Change Mitigation*, 2013.

[16] M. Birch and R. Cary, "Elemental carbon-based method for monitoring occupational exposures to particulate diesel exhaust," *Aerosol Science and Technology*, vol. 25, pp. 221-241, 1996.

[17] L.-H. Young, Y.-J. Liou, M.-T. Cheng, J.-H. Lu, H.-H. Yang, Y. I. Tsai, *et al.*, "Effects of biodiesel, engine load and diesel particulate filter on nonvolatile particle number size distributions in heavy-duty diesel engine exhaust," *Journal of hazardous materials*, vol. 199, pp. 282-289, 2012.

[18] E. Al Katheeri, F. Al Jallad, and M. Al Omar, "Assessment of gaseous and particulate pollutants in the ambient air in Al Mirfa City, United Arab Emirates," *Journal of Environmental Protection*, vol. 3, p. 640, 2012.

[19] J. P. Engelbrecht, E. V. McDonald, J. A. Gillies, R. "Jay" Jayanty, G. Casuccio, and A. W. Gertler, "Characterizing mineral dusts and other aerosols from the Middle East—Parts 1 and 2: Grab samples and re-suspensions," *Inhalation toxicology*, vol. 21, pp. 327-336, 2009.

[20] J. P. Engelbrecht, E. V. McDonald, J. A. Gillies, and A. W. Gertler, "Department of Defense Enhanced Particulate Matter Surveillance Program (EPMSP)," DESERT RESEARCH INST RENO NV2008.

[21] A. A. Al-Taani, Y. Nazzal, F. M. Howari, and A. Yousef, "Long-term trends in ambient fine particulate matter from 1980 to 2016 in United Arab Emirates," *Environmental monitoring and assessment*, vol. 191, p. 143, 2019.

[22] H. Al-Thani, M. Koc, and R. J. Isaifan, "Investigations on deposited dust fallout in Urban Doha: characterization, source apportionment and mitigation," *Environ. Ecol. Res*, vol. 6, pp. 493-506, 2018.

[23] M. Arashiro and D. Leith, "Precision of PM measurements with the UNC passive aerosol sampler," *Journal of aerosol science*, vol. 57, pp. 181-184, 2013.

[24] J. P. Engelbrecht, E. V. McDonald, J. A. Gillies, R. Jayanty, G. Casuccio, and A. W. Gertler, "Characterizing mineral dusts and other aerosols from the Middle East—part 1: ambient sampling," *Inhalation Toxicology*, vol. 21, pp. 297-326, 2009.

[25] J. Reid, D. Westphal, E. Reid, A. Walker, M. Liu, S. Miller, *et al.*, "The United Arab Emirates Unified Aerosol Experiment (UAE2)," NAVAL RESEARCH LAB MONTEREY CA MARINE METEOROLOGY DIV2006.

[26] S. Al-Salem, "An overview of the PM10 pollution problem in Fahaheel urban area, Kuwait," *Emirates Journal of Engineering Research*, vol. 13, pp. 1-9, 2008.

[27] N. Alattar and J. Yousif, "Evaluating Particulate Matter (PM2. 5 and PM10) Impact on Human Health in Oman Based on a Hybrid Artificial Neural Network and Mathematical Models," in *2019 International Conference on Control, Artificial Intelligence, Robotics & Optimization (ICCAIRO)*, 2019, pp. 129-135.

[28] N. M. Hamdan and H. Alawadhi, "X-ray diffraction as a major tool for the analysis of PM 2.5 and PM 10 aerosols," *Powder Diffraction*, pp. 1-6, 2020.

[29] N. M. Hamdan, H. Alawadhi, and N. Jisrawi, "Particulate matter pollution in the United Arab Emirates: Elemental analysis and phase identification of fine particulate pollutants," in *Proceedings of the 2nd World Congress on New Technologies (NewTech'16) Budapest, Hungary–August*, 2016, pp. 18-19.

[30] N. M. Hamdan, H. Alawadhi, and N. Jisrawi, "Elemental and Chemical Analysis of PM10 and PM2. 5 Indoor and Outdoor Pollutants in the UAE," *International Journal of Environmental Science and Development*, vol. 6, p. 566, 2015.

[31] L. Samek, Z. Stegowski, and L. Furman, "Preliminary PM2. 5 and PM10 fractions source apportionment complemented by statistical accuracy determination," *Nukleonika*, vol. 61, pp. 75-83, 2016.

[32] A. Petzold, J. A. Ogren, M. Fiebig, P. Laj, S. Li, U. Baltensperger, *et al.*, "Recommendations for reporting" black carbon" measurements," 2013.

[33] D. D. Cohen, G. Taha, E. Stelcer, D. Garton, and G. Box, "The measurement and sources of fine particle elemental carbon at several key sites in NSW over the past eight years," in *Proceedings of 15th International Clean Air and Environment Conference*, 2000, pp. 485-490.

[34] R. Zalakeviciute, J. López-Villada, and Y. Rybarczyk, "Contrasted effects of relative humidity and precipitation on urban PM2. 5 pollution in high elevation urban areas," *Sustainability*, vol. 10, p. 2064, 2018.

[35] Y. Cheng, K.-b. He, Z.-y. Du, M. Zheng, F.-k. Duan, and Y.-l. Ma, "Humidity plays an important role in the PM2. 5 pollution in Beijing," *Environmental pollution*, vol. 197, pp. 68-75, 2015.

[36] timeanddate. (2020, August 25). *Climate & Weather Averages in Sharjah, Sharjah, United Arab Emirates*. Available: https://www.timeanddate.com/weather/united-arab-emirates/sharjah/climate

[37] B. Chen, A. Andersson, M. Lee, E. N. Kirillova, Q. Xiao, M. Kruså, *et al.*, "Source forensics of black carbon aerosols from China," *Environmental science & technology*, vol. 47, pp. 9102-9108, 2013.

[38] R. Kumar, M. Barth, V. Nair, G. Pfister, S. Suresh Babu, S. Satheesh, *et al.*, "Sources of black carbon aerosols in South Asia and surrounding regions during the Integrated Campaign for Aerosols, Gases and Radiation Budget (ICARB)," *Atmospheric Chemistry and Physics (Online)*, vol. 15, 2015.

[39] X. Song, L. Shao, Q. Zheng, and S. Yang, "Characterization of crystalline secondary particles and elemental composition in PM 10 of North China," *Environmental earth sciences*, vol. 74, pp. 5717-5727, 2015.

[40] J. H. Seinfeld and S. N. Pandis, *Atmospheric chemistry and physics: from air pollution to climate change*: John Wiley & Sons, 2016.

[41] H. Liao, P. J. Adams, S. H. Chung, J. H. Seinfeld, L. J. Mickley, and D. J. Jacob, "Interactions between tropospheric chemistry and aerosols in a unified general circulation model," *Journal of Geophysical Research: Atmospheres*, vol. 108, pp. AAC 1-1-AAC 1-23, 2003.

[42] M. Manousakas, H. Papaefthymiou, E. Diapouli, A. Migliori, A. Karydas, I. Bogdanovic-Radovic, *et al.*, "Assessment of PM2. 5 sources and their corresponding level of uncertainty in a coastal urban area using EPA PMF 5.0 enhanced diagnostics," *Science of the Total Environment*, vol. 574, pp. 155-164, 2017.

[43] M. Manousakas, E. Diapouli, H. Papaefthymiou, V. Kantarelou, C. Zarkadas, A. C. Kalogridis, *et al.*, "XRF characterization and source apportionment of PM10 samples collected in a coastal city," *X-Ray Spectrometry*, vol. 47, pp. 190-200, 2018.

[44] M. Bove, P. Brotto, F. Cassola, E. Cuccia, D. Massabò, A. Mazzino, *et al.*, "An integrated PM2. 5 source apportionment study: positive matrix factorisation vs. the chemical transport model CAMx," *Atmospheric environment*, vol. 94, pp. 274-286, 2014.

[45] F. Mazzei, A. D'alessandro, F. Lucarelli, S. Nava, P. Prati, G. Valli, *et al.*, "Characterization of particulate matter sources in an urban environment," *Science of the Total Environment*, vol. 401, pp. 81-89, 2008.

[46] L. Yao, L. Yang, Q. Yuan, C. Yan, C. Dong, C. Meng, *et al.*, "Sources apportionment of PM2. 5 in a background site in the North China Plain," *Science of the Total Environment*, vol. 541, pp. 590-598, 2016.

[47] H. gon Ryou, J. Heo, and S.-Y. Kim, "Source apportionment of PM10 and PM2. 5 air pollution, and possible impacts of study characteristics in South Korea," *Environmental Pollution*, vol. 240, pp. 963-972, 2018.

[48] EU-Commission. (2020, March 7). *Air Quality Standards*. Available: https://ec.europa.eu/environment/air/quality/standards.htm

[49] M. Viana, T. Kuhlbusch, X. Querol, A. Alastuey, R. Harrison, P. Hopke, *et al.*, "Source apportionment of particulate matter in Europe: a review of methods and results," *Journal of aerosol science*, vol. 39, pp. 827-849, 2008.

[50] J.-H. Jeong, Z.-H. Shon, M. Kang, S.-K. Song, Y.-K. Kim, J. Park, *et al.*, "Comparison of source apportionment of PM2. 5 using receptor models in the main hub port city of East Asia: Busan," *Atmospheric Environment*, vol. 148, pp. 115-127, 2017.

[51] A. Nigam, W. Welch, J. Wayne Miller, and D. Cocher III, "Effect of fuel sulphur content and control technology on PM emission from ship's auxiliary engine," in *Proceeding international aerosol conference, St. Paul, USA*, 2006, pp. 10-15.

[52] A. Iijima, K. Sato, K. Yano, H. Tago, M. Kato, H. Kimura, *et al.*, "Particle size and composition distribution analysis of automotive brake abrasion dusts for the evaluation of antimony sources of airborne particulate matter," *Atmospheric Environment*, vol. 41, pp. 4908-4919, 2007.

[53] I. Salma and W. Maenhaut, "Changes in elemental composition and mass of atmospheric aerosol pollution between 1996 and 2002 in a Central European city," *Environmental pollution,* vol. 143, pp. 479-488, 2006.

[54] J. Lyman and R. H. Fleming, "Composition of sea water," *J Mar Res,* vol. 3, pp. 134-146, 1940.

[55] X. Wang, X. Bi, G. Sheng, and J. Fu, "Chemical composition and sources of PM10 and PM2. 5 aerosols in Guangzhou, China," *Environmental monitoring and Assessment,* vol. 119, pp. 425-439, 2006.

[56] C.-S. Zhu, J.-J. Cao, Z.-X. Shen, S.-X. Liu, T. Zhang, Z.-Z. Zhao, *et al.*, "Indoor and outdoor chemical components of PM2. 5 in the rural areas of Northwestern China," *Aerosol Air Qual. Res,* vol. 12, pp. 1157-1165, 2012.

[57] R. A. Duce, G. L. Hoffman, and W. H. Zoller, "Atmospheric trace metals at remote northern and southern hemisphere sites: pollution or natural?," *Science,* vol. 187, pp. 59-61, 1975.

[58] J. Feng, H. Yu, X. Su, S. Liu, Y. Li, Y. Pan, *et al.*, "Chemical composition and source apportionment of PM2. 5 during Chinese Spring Festival at Xinxiang, a heavily polluted city in North China: Fireworks and health risks," *Atmospheric Research,* vol. 182, pp. 176-188, 2016.

[59] L. Wu, X.-S. Luo, H. Li, L. Cang, J. Yang, J. Yang, *et al.*, "Seasonal Levels, Sources, and Health Risks of Heavy Metals in Atmospheric PM2. 5 from Four Functional Areas of Nanjing City, Eastern China," *Atmosphere,* vol. 10, p. 419, 2019.

[60] A. M. Helmenstine. (2020, May 18). *Chemical Composition of the Earth's Crust - Elements*. Available: https://www.thoughtco.com/chemical-composition-of-earths-crust-elements-607576

[61] R. Rudnick and S. Gao, "Composition of the continental crust," *The crust,* vol. 3, pp. 1-64, 2003.

[62] Dubai-Online. (2020 April 20). *Dubai Population and Demographics*. Available: https://www.dubai-online.com/essential/uae-population-and-demographics/

[63] P. Pant, A. Shukla, S. D. Kohl, J. C. Chow, J. G. Watson, and R. M. Harrison, "Characterization of ambient PM2. 5 at a pollution hotspot in New Delhi, India and inference of sources," *Atmospheric Environment,* vol. 109, pp. 178-189, 2015.

[64] J. C. Chow, J. G. Watson, H. Kuhns, V. Etyemezian, D. H. Lowenthal, D. Crow, *et al.*, "Source profiles for industrial, mobile, and area sources in the Big Bend Regional Aerosol Visibility and Observational study," *Chemosphere,* vol. 54, pp. 185-208, 2004.

[65] P. Fu, K. Kawamura, C. Pavuluri, T. Swaminathan, and J. Chen, "Molecular characterization of urban organic aerosol in tropical India: contributions of primary emissions and secondary photooxidation," *Atmospheric Chemistry and Physics,* vol. 10, pp. 2663-2689, 2010.

[66] S. Overdahl. (2020, August 25). *CONSTRUCTIONUAE takes the lead on diesel*. Available: https://meconstructionnews.com/6444/uae-takes-the-lead-on-diesel

[67] A. Ianniello, F. Spataro, G. Esposito, I. Allegrini, M. Hu, and T. Zhu, "Chemical characteristics of inorganic ammonium salts in PM 2.5 in the atmosphere of Beijing (China)," *Atmospheric Chemistry and Physics,* vol. 11, pp. 10803-10822, 2011.

[68] export.gov. (2019, September 1). *United Arab Emirates - Oil and Gas Field Machinery and Services*. Available: https://www.export.gov/apex/article2?id=United-Arab-Emirates-Energy-Power

[69] P. Satsangi and S. Yadav, "Characterization of PM 2.5 by X-ray diffraction and scanning electron microscopy–energy dispersive spectrometer: its relation with different pollution sources," *International Journal of Environmental Science and Technology,* vol. 11, pp. 217-232, 2014.

Table 1: Dust events during the sampling campaign.

#	Date	$PM_{2.5}$ Concentration (µg/m^3)	PM_{10} Concentration (µg/m^3)	Wind speed (km/h)	Wind Direction
1	02/20/2018	42	290	28	W
2	04/17/2018	68	325	15	NNW
3	05/01/2018	68	195	13, 17, 13	S, WNW, W
4	05/08/2018	58	243	16	NW
5	06/01/2018	80	218	17	NW
6	06/05/2018	56	228	19	NW
7	06/08/2018	97	195	15	W
8	06/26/2018	62	239	21	W
9	06/29/2018	60	319	22	E
10	07/03/2018	85	292	12	NNW
11	07/06/2018	61	341	27	E
12	07/10/2018	82	296	17, 12	SSE, NW
13	07/31/2018	146	676	7, 8, 17	S, SE, NW
14	08/10/2018	72	294	21	E
15	08/17/2018	57	238	16, 16	SSE, WNE

Table 2: Correlation coefficients among the measured elemental concentrations.

	Na_2O	MgO	Al_2O_3	SiO_2	P_2O_5	S	Cl	K_2O	CaO	TiO_2	VO_2	Cr_2O_3	MnO	Fe_2O_3	NiO	CuO	ZnO	Rb_2O	SrO	ZrO_2	BaO	PbO
Na_2O	1.00	0.30	0.13	0.13	0.26	-0.23	0.54	0.08	0.26	0.11	-0.07	0.10	0.08	0.09	0.06	-0.15	-0.14	0.09	0.28	-0.14	-0.14	-0.01
MgO		1.00	0.86	0.02	0.78	-0.17	0.56	0.77	0.94	0.82	0.09	0.83	0.85	0.88	0.64	0.08	0.24	0.64	0.83	0.58	0.45	0.13
Al_2O_3			1.00	0.38	0.62	-0.04	0.35	0.92	0.81	0.95	0.19	0.77	0.87	0.96	0.61	0.14	0.28	0.77	0.64	0.60	0.42	0.07
SiO_2				1.00	0.13	-0.41	0.16	-0.30	0.01	-0.31	-0.32	-0.01	-0.15	-0.22	-0.16	-0.06	0.01	-0.30	0.01	-0.02	0.11	0.09
P_2O_5					1.00	-0.24	0.55	0.53	0.79	0.63	0.11	0.71	0.65	0.67	0.55	0.08	0.17	0.46	0.72	0.50	0.48	0.07
S						1.00	-0.29	0.05	-0.10	-0.03	0.40	0.01	-0.02	-0.04	0.25	-0.06	0.15	0.10	-0.08	-0.04	-0.15	-0.06
Cl							1.00	*0.22*	*0.58*	*0.33*	-0.16	0.37	0.33	0.36	0.18	0.14	0.04	0.27	0.48	0.16	0.13	0.04
K_2O								1.00	0.75	0.90	0.30	0.75	0.86	0.93	0.65	0.06	0.36	0.79	0.54	0.66	0.49	0.14
CaO									1.00	0.82	0.12	0.89	0.83	0.89	0.69	0.04	0.28	0.63	0.88	0.54	0.43	0.06
TiO_2										1.00	0.16	0.79	0.86	0.95	0.61	0.11	0.38	0.76	0.63	0.63	0.45	0.07
VO_2											1.00	0.24	0.30	0.22	0.75	0.03	0.22	0.20	0.14	0.16	0.20	0.05
Cr_2O_3												1.00	0.91	0.88	0.79	0.11	0.46	0.64	0.74	0.63	0.45	0.16
MnO													1.00	0.95	0.76	0.15	0.51	0.73	0.64	0.72	0.52	0.25
Fe_2O_3														1.00	0.71	0.14	0.43	0.78	0.68	0.69	0.50	0.15
NiO															1.00	0.07	0.41	0.53	0.61	0.47	0.40	0.11
CuO																1.00	0.39	0.43	0.00	0.24	0.12	0.49
ZnO																	1.00	0.44	0.12	0.49	0.41	0.46
Rb_2O																		1.00	0.45	0.56	0.42	0.23
SrO																			1.00	0.33	0.32	-0.07
ZrO_2																				1.00	0.61	0.35
BaO																					1.00	0.35
PbO																						1.00

Table 3: Pb concentration in the premises of a car battery recycling plant.

Sample date	Pb Concentration (μg/m^3)
Working day 1 (04/21/2018)	0.67
Working Day 2 (04/29, 2018)	0.81
Weekend (No recycling) (05/31/2018)	0.13

1 **Table 4:** Summary of source tags for various elements.

Natural		Anthropogenic	
Crustal	Al, Si, Ca, K, P, Fe, Ti, Mn, Mg, Na, Cr, Sr	Ships	V, Ni
Sea Salt	Na, Cl	Road Traffic	Ba, Zn, Fe, Cu, BC (Ca, Al, Si)
		Secondary	S
		Car battery recycling	Pb
		Unknown	Rb, Zr, (Sr)

2

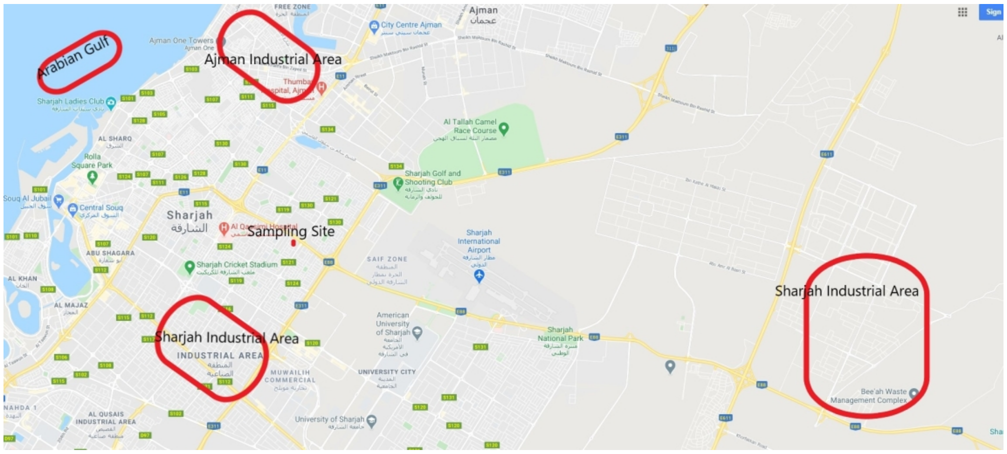

Figure 1. Map of the sampling site in Sharjah, showing three industrial areas, Sharjah Airport and the Arabian Gulf in the vicinity

486x217mm (96 x 96 DPI)

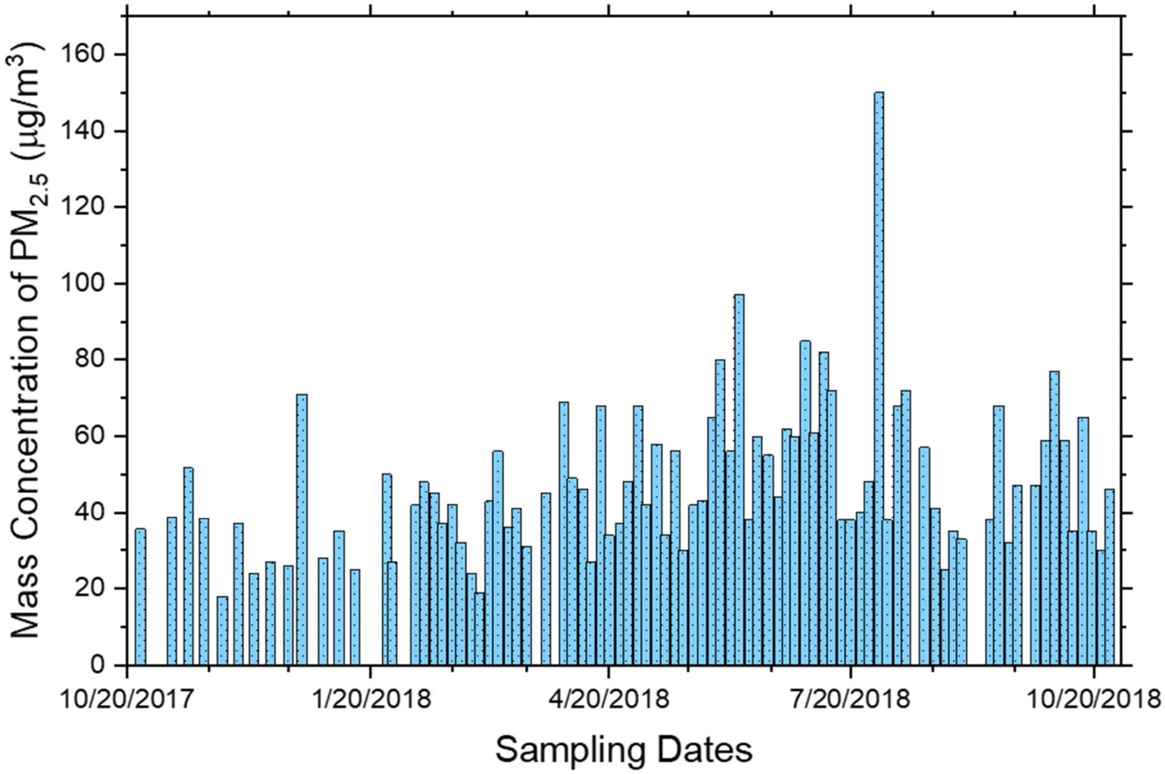

Figure 2. Variation of the mass concentrations in $\mu g/m^3$ for each of the $PM_{2.5}$ samples collected over the sampling campaign period.

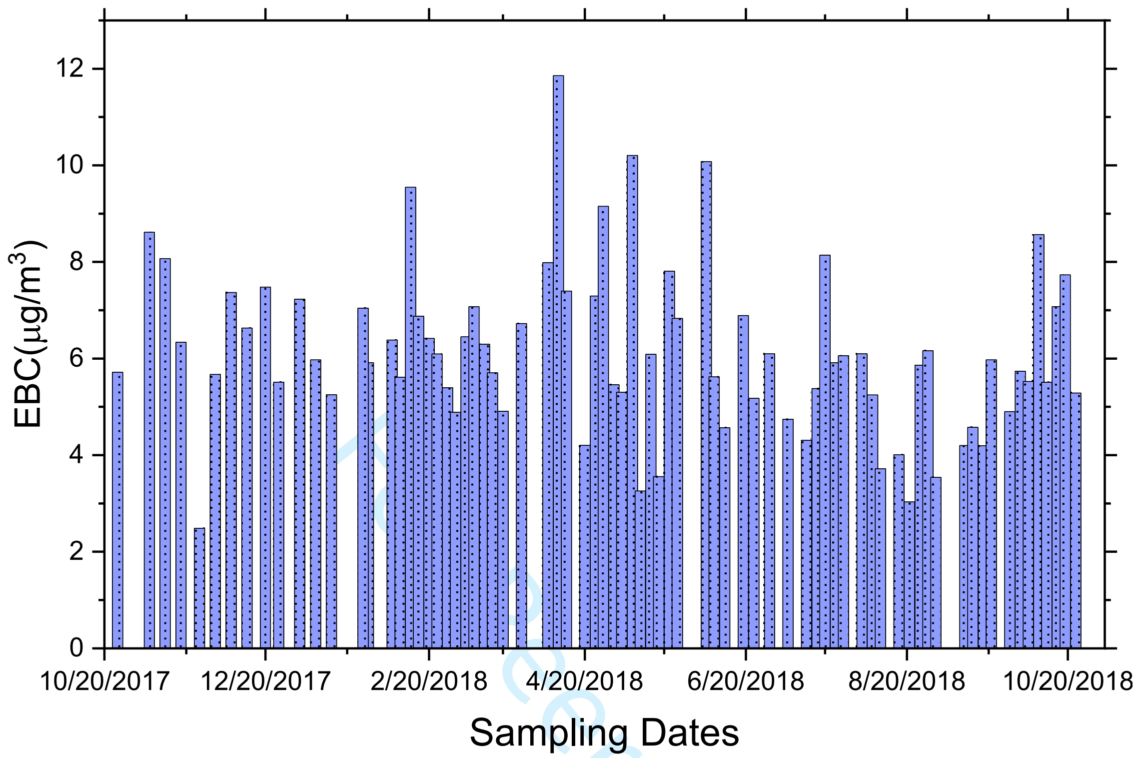

Figure 3. eBC content of $PM_{2.5}$ for the campaign period.

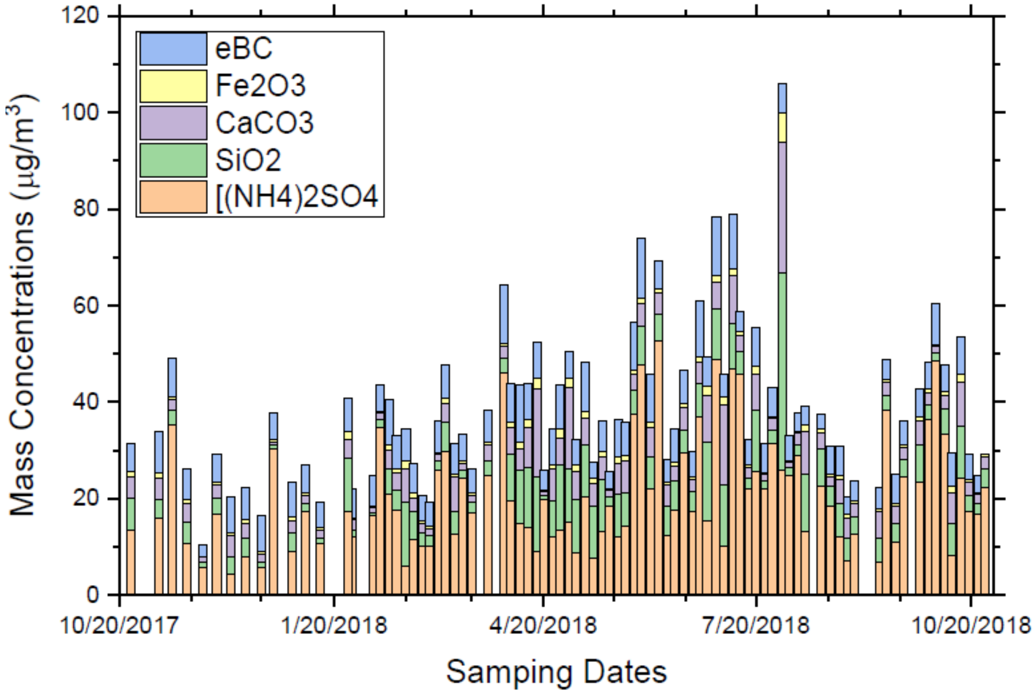

Figure 4. Variation of Ca, Si, Fe and eBC concentrations with time.

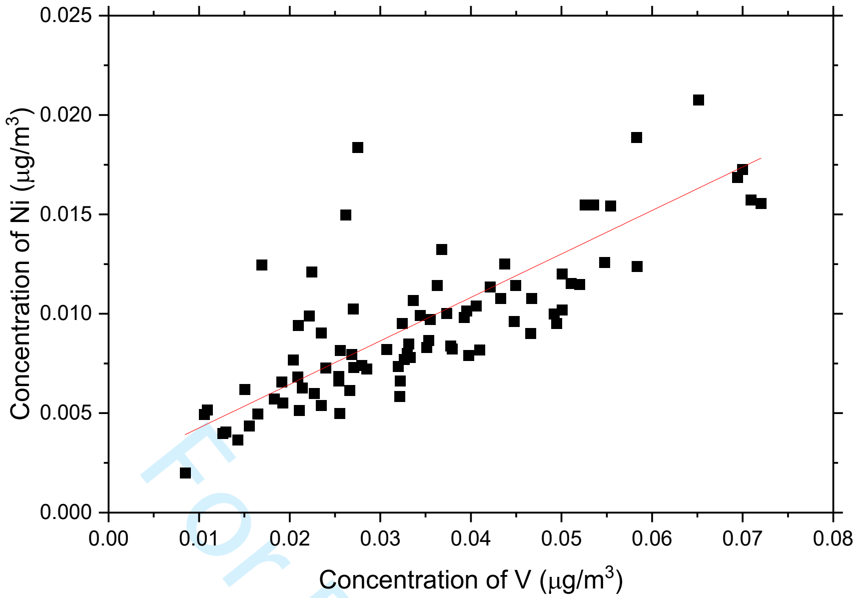

Figure 5. Scatter plot of concentration variation for Ni and V, showing good correlation (R = 0.75) between these two elements.

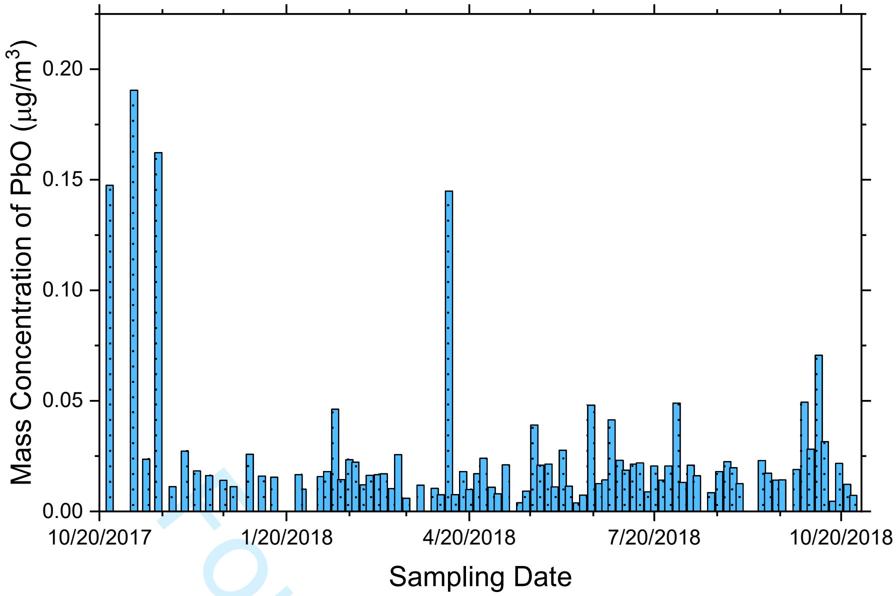

Figure 6. Concentration variation of Pb content for the sampling days.

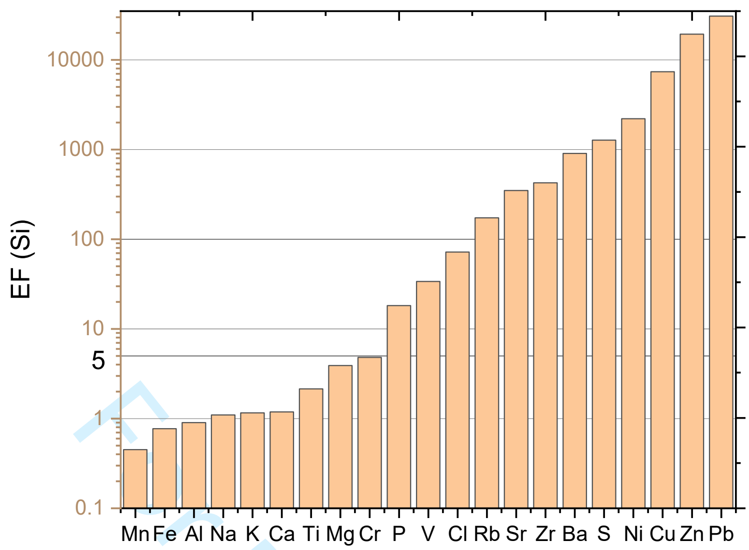

(a)

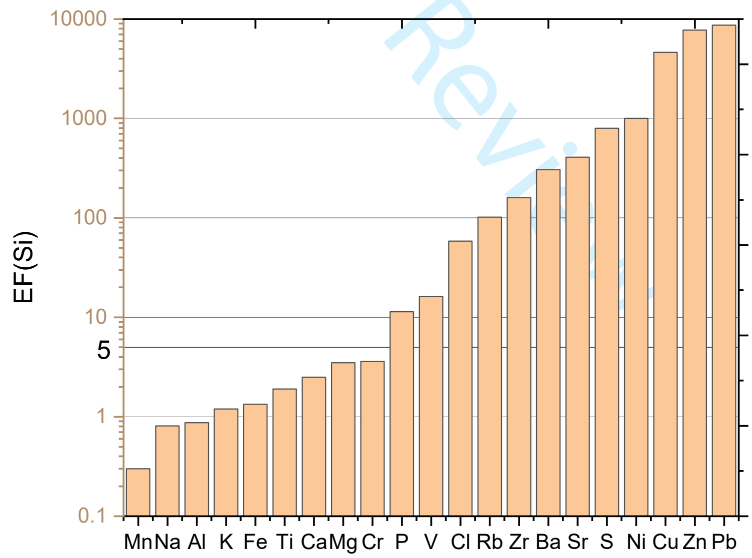

(b)

Figure 7. EF of the elements (a) for the cold season and (b) for the hot season.

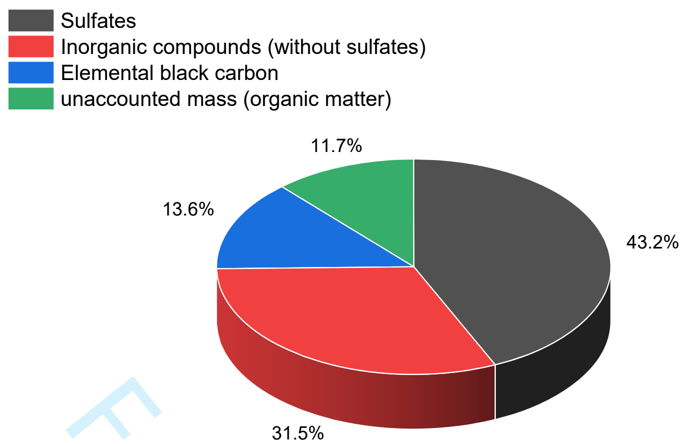

Figure 8: Preliminary contributions of the average of $PM_{2.5}$ mass

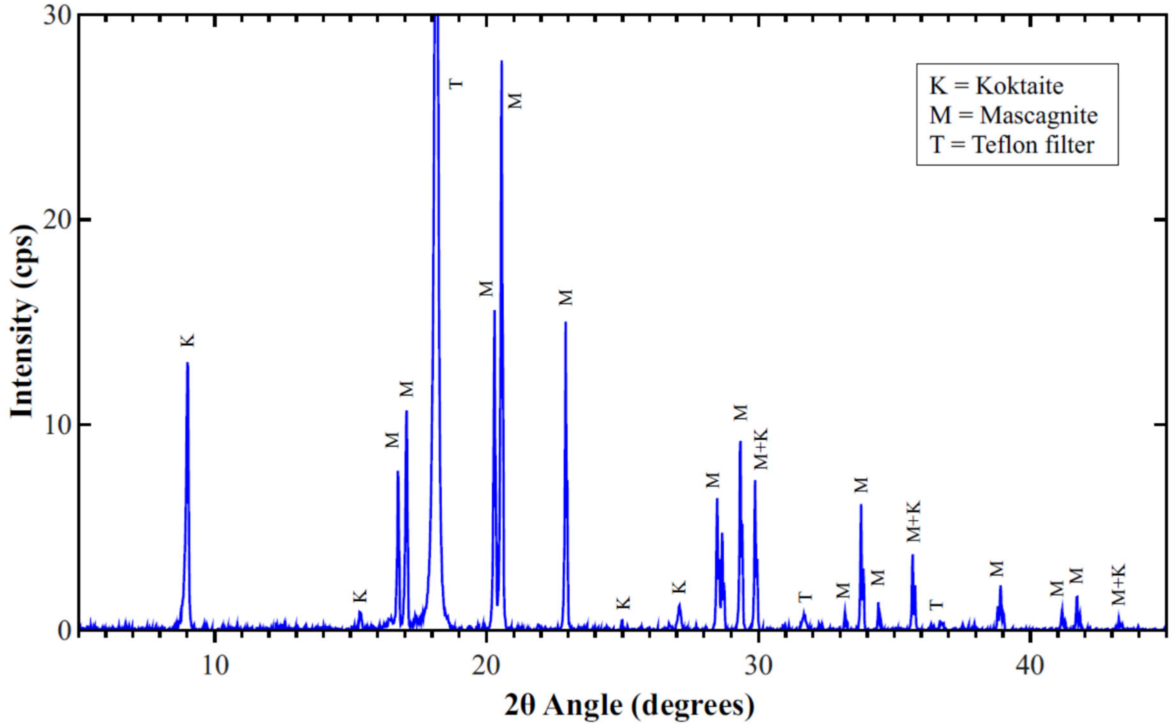

Figure 9. XRD pattern for filter 80, sampled on October 5, 2018. Most of the tested $PM_{2.5}$ samples show the same phases.

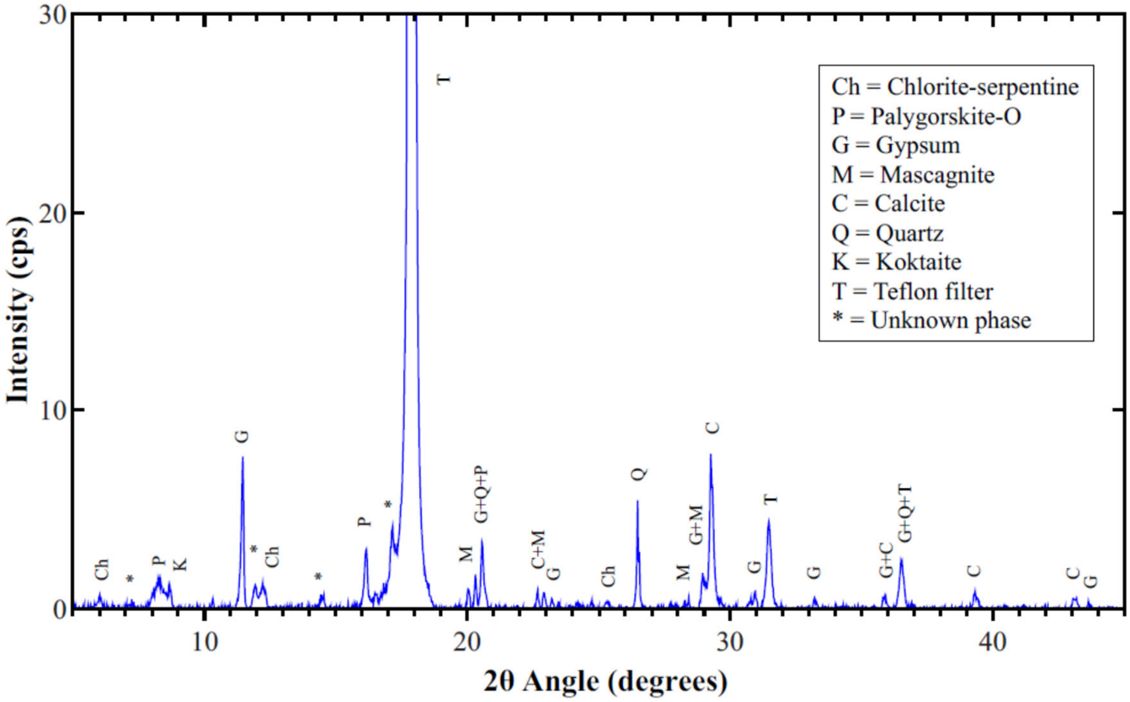

Figure 10. XRD pattern for filter 35, sampled on April 17, 2018, a dusty day.

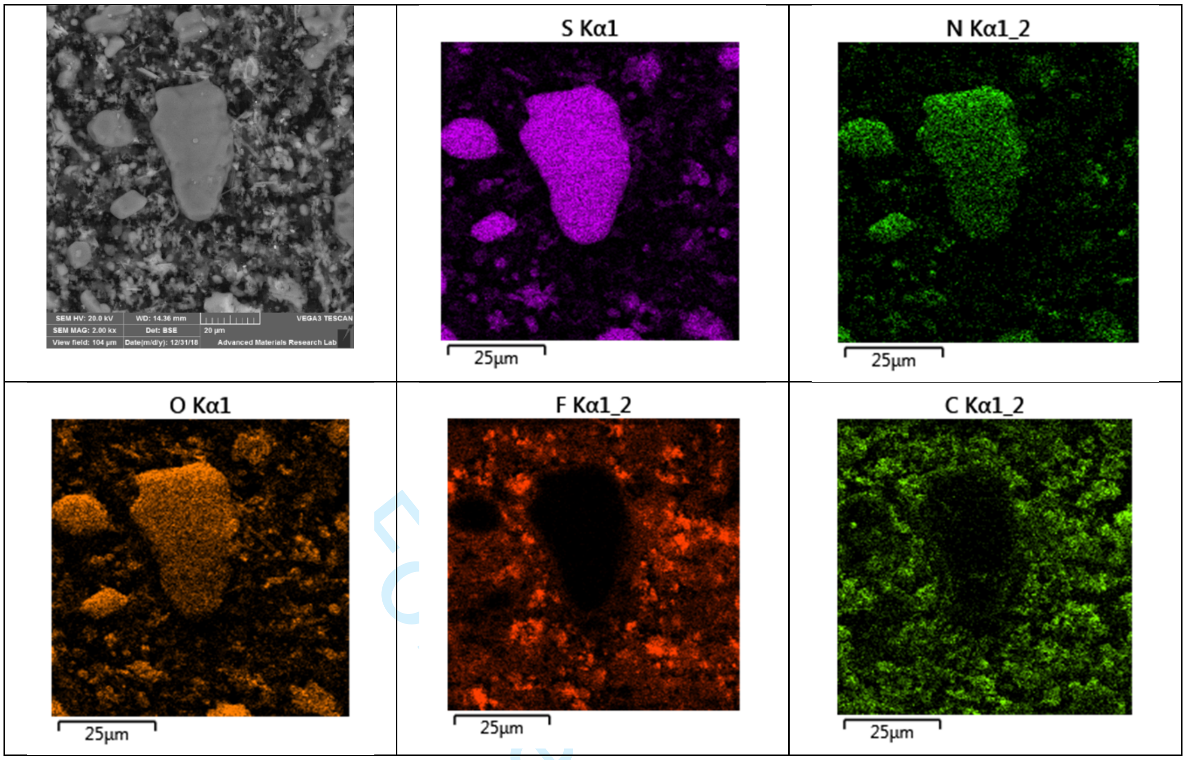

Figure 11. SEM micrograph (2000x magnification) and elemental maps of S, N, O, F and C for $PM_{2.5}$ sample 80, collected on October 5, 2018.

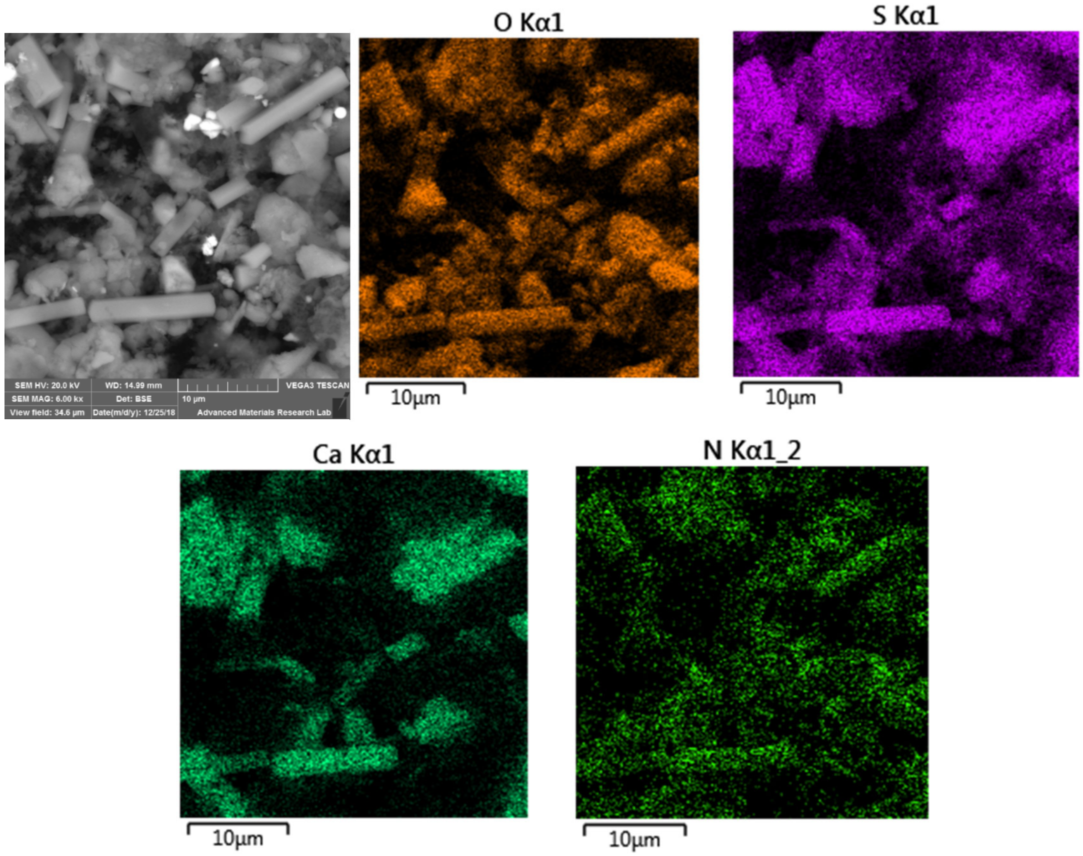

Figure 12. SEM micrograph (6000x magnification) and elemental maps of Ca, S, N and O for PM_{10} sample 67, collected on October 5, 2018.

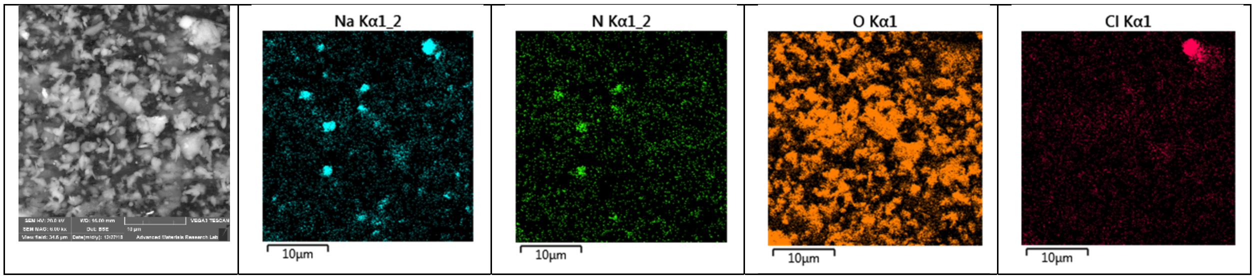

Figure 13. SEM micrograph and elemental maps for sample 21, collected on February 20, 2018, showing correlations between Na and Cl for one crystal (upper right corner) and no correlation with oxygen. Several other crystals show correlations among Na, N and O.